INTERNATIONAL JOURNAL OF HYDROGEN ENERGY XXX (2015) 1–10

Available online at www.sciencedirect.com

ScienceDirect

journal homepage: www.elsevier.com/locate/he

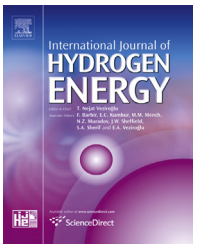

Terminal solid solubility determinations in the H–Ti system

P. Vizcaíno [a,b,*], I.A. Lopez Vergara [b], A.D. Banchik [a], J.P. Abriata [c]

[a] Centro Atómico Ezeiza, Comisión Nacional de Energía Atómica, Pres. J. Gonzáles y Aragón 15, B1802AYA, Argentina

[b] Universidad Nacional La Matanza, San Justo, Pcia. de Bs. As., Argentina

[c] Independent Consultant, S. C. de Bariloche, Río Negro, Argentina

ARTICLE INFO

Article history:
Received 16 December 2014
Received in revised form
9 June 2015
Accepted 10 June 2015
Available online xxx

Keywords:
Hydrogen
Solubility
Titanium
Hydride phases
Differential scanning calorimetry

ABSTRACT

The terminal solid solubility of hydrogen in titanium was measured by differential scanning calorimetry in the concentration range of 0.3–4.1 at.% which practically corresponds to the whole solubility range of hydrogen in α-Ti. The solvus enthalpy obtained in this range from the overall data set was 22.8 ± 0.5 kJ/molH. However, a more careful analysis of the experimental results shows that the solubility curve has two different behaviors as a function of concentration. In the high concentration range 1.4–4.1 at.% a solvus enthalpy of 29.0 ± 1.5 kJ/molH was obtained representing the $\alpha/\alpha+\delta$ equilibrium boundary. In the low concentration range, 0.3 at.% to 1.4 at.%, the slope was noticeably lower with 24.2 ± 1.5 kJ/molH for the solvus enthalpy. This last value should correspond to the $[\alpha]/[\alpha+\gamma]$ equilibrium curve. Although it is possible this value might be influenced by the presence of tiny amounts of the now metastable δ phase—as its presence is revealed by X-ray diffraction analysis – anyway it is consistent with a $\alpha+\delta \leftrightarrow \gamma$ peritectoid reaction temperature of 168 °C obtained from the literature.

The eutectoid $\alpha+\delta \leftrightarrow \beta$ decomposition temperature was determined using samples of high hydrogen contents, ranging from 9 to 11.0 at.%. This temperature was determined to be 319.9 ± 1 °C from the analysis of the DSC diagrams. The solubility limit $[\alpha]/[\alpha+\delta]$ at this eutectoid reaction was estimated to be 5.44 ± 0.27 at.%.

The present results are believe to provide a closer approximation to the solubility values of H in α-Ti as presently reported in the literature.

Introduction

In spite of the technological importance of an accurate knowledge of the solvus line for hydrogen in titanium-based alloys, there is lack of data for this region of the H–Ti phase diagram. In the last revision of phase stability in the H–Ti system made by Manchester [1] all the existing data regarding the solvus region were compiled. The solvus region was essentially assessed by means of the internal friction measurements made by Köster [2] and the resistivity data of Paton et al. [3] and Vitt [4]. These sets of data were analyzed by Luo [5]

* *Corresponding author*. Centro Atómico Ezeiza, Comisión Nacional de Energía Atómica, Pres. J. Gonzáles y Aragón 15, B1802AYA, Argentina.
E-mail address: vizcaino@cae.cnea.gov.ar (P. Vizcaíno).

http://dx.doi.org/10.1016/j.ijhydene.2015.06.058

adding to them his own calorimetric measurements. The solvus enthalpy calculated through the slope of the Van't Hoff plot by Luo [5] was $\Delta H_{solv} = 22.9$ kJ/molH. This value is different from those obtained by Paton [3] and Vitt [4], both close to $\Delta H_{solv} = 18.7$ kJ/molH. Nevertheless, the whole data set is rather small and in some cases dissolution and precipitation data were both used for the solvus line, neglecting hysteresis effects [4,5]. The limited number of data points makes it difficult to be reasonably sure about the accuracy of the solvus line and solvus enthalpy. Indeed, the approximation of a common solvus line was assumed for both, $[\alpha]/[\alpha+\gamma]$ and $[\alpha]/[\alpha+\delta]$ boundary limits [1]. In general, the accuracy of the experimental determinations improves as the hydrogen concentration increases. Probably ought to this most of the literature data corresponds to concentration ranges above 1 at.% and data are scarce for lower concentration values [2,5,6]. The temperature of terminal solid solubility for most data found in the literature are over 168 °C, that is, higher than the accepted $\alpha+\gamma \rightarrow \alpha+\delta$ transition temperature [1]. The fewer data existing below this temperature show a significant scatter, making it virtually impossible to differentiate between the boundaries $[\alpha]/[\alpha+\gamma]$ and $[\alpha]/[\alpha+\delta]$ along the solvus line, where in principle the enthalpies of dissolution should be different.

In the described framework, the aim of the present work was to improve the quality of the data of the solvus in the Ti–H system, making measurements along the solubility interval, trying to cover the whole solvus concentration range where the reactions $\alpha \rightarrow \alpha+\gamma$ and $\alpha \rightarrow \alpha+\delta$ take place, but paying particular attention to the peritectoid reaction:

$$\alpha\text{–Ti (H)} + \delta\ (X \sim 2,\ 66.7\ \text{at.\%}) \leftrightarrow \gamma\ (X \sim 1,\ 50\ \text{at.\%});\ \text{at } 168\ ^\circ\text{C},$$

where X is the atomic ratio (H/Ti). With this aim the approach was made in the present work using a highly sensitive technique as differential scanning calorimetry, DSC, for a large number of samples containing from 0.3 to 4.1 at.%.

The calorimetric results were complemented by X-ray diffraction experiments used for γ and δ hydride phases recognition. For these experiments several samples in the whole hydrogen concentration range from 0.3 to 4.1 at.% hydrogen were prepared. These samples were annealed and cooled under different conditions. The results showed a high proportion of the γ phase at room temperature for the low hydrogen samples. However, it was found that the amount of the γ phase decreases as the hydrogen content increases with the appearance of the δ phase which is metastable at room temperature in this concentration range. We conclude that our DSC and X-ray diffraction results are mutually consistent and give adequate support to the interpretations made in the present work.

Materials

The samples were taken from a hot rolled titanium rod grade 2. From this rod, discs of 2 mm thick and 25.4 mm in diameter were cut. The discs were thermally treated at 900 °C during 45 min under vacuum (1.33×10^{-3} Pa) to eliminate the hot rolling microstructure by generating a new homogeneous one, formed by equiaxed grains. The grain size was of 100 μm. The chemical composition is shown in Table 1.

Hydrogen incorporation

Hydrogen was incorporated in two stages:

First, a hydride surface layer was deposited over the discs by the cathodic charge technique. Secondly, hydrogen was diffused into the bulk by annealing the discs at 400 °C during 24 h.

The cathodic charge was made using an electrolytic cell by circulating through the sample a current density of 0.15 A/cm^2. The electrolytic solution was prepared with a mixture of glycerin (50%) and phosphoric acid (50%). The samples were submerged in this solution (cathode) and the circuit was closed performing a joint by welding (using a point welding machine) the sample to a platinum wire. The charging periods varied between 4 h and 100 h. As a result, optical microscopy observations revealed hydride layers from a few microns to 50 microns covering the sample surfaces. Following this procedure, hydrogen contents within the interval 0.3 at.% to 11.0 at.% were obtained. Finally, after an annealing of 24 h at 400 °C, the discs were polished with SiC paper to remove the oxide layer and any remaining hydride on the sample surface.

Samples for DSC and hydrogen determination

For the DSC experiments, about 50 samples of 4 mm × 4 mm × 1.8 mm were cut from the hydrided and homogenized discs. After the calorimetric program finished, the hydrogen content was measured for each sample. They were polished again to eliminate the oxide layer formed during the DSC runs, washed with acetone and dried with hot air. These hydrogen contents were determined with a hydrogen meter LECO RH-404. The experimental error of these determinations is ±4 wppm for the samples with hydrogen content smaller than 100 wppm and ±4% of the measured value for higher concentrations.

Samples for X-ray diffraction

Some of the discs were selected for X-ray measurements. The aim of these experiments was to pursue the reaction $\alpha+\gamma \rightarrow \alpha+\delta$ and its reverse $\alpha+\delta \rightarrow \alpha+\gamma$. Hence, two sets of samples were prepared.

Samples with hydrogen contents above the solid solubility range were produced. One sample containing 11.0 at.% was annealed 24 h at 400 °C under a N_2 (99.99% pure) atmosphere and cooled in furnace. Another sample containing ~5.0 at.%

Table 1 – Chemical composition of a Ti grade 2 rod.

Element	Concentration (wt%)
O	0.115
Fe	0.039
C	0.004
N	0.007
H	0.0025
Ti	up to 100%

Please cite this article in press as: Vizcaíno P, et al., Terminal solid solubility determinations in the H–Ti system, International Journal of Hydrogen Energy (2015), http://dx.doi.org/10.1016/j.ijhydene.2015.06.058

was annealed at 155 °C for a week, that is, about 15 °C below the peritectoid $\alpha + \gamma \rightarrow \alpha + \delta$ reaction temperature.

The surface of both samples were mechanically polished and chemically pickled to obtain a good reflecting surface for the X-rays.

A powder sample containing 11.0 at.% was also used. The powder was obtained by filing a solid hydrided sample. It was annealed 1 h at 600 °C under a N_2 (99.99% pure) atmosphere and then cooled in air. After this, it was pickled in a solution of water (50%) nitric acid (45%) and hydrofluoric acid (5%) to eliminate any oxide layer formed during the cooling.

Samples with low hydrogen contents corresponding to the solid solubility range were also produced. For these samples a hydride layer of a few microns (1–3 μm) was diffused into the bulk by heating the samples up to 100 °C, 150 °C and 250 °C at 1 °C/min and cooling at the same rate, under N_2 atmosphere. Following this procedure, samples ranging from 0.31 at.% to 0.67 at.% were obtained. After this, their surfaces were polished with SiC paper and chemically pickled for the X-rays experiments.

Experimental

Differential scanning calorimetry

The temperatures of terminal solid solubility on dissolution, TTSS, which are considered a good approximation to the equilibrium values [7,8], were determined using a thermal flux differential scanning calorimeter Shimadzu DSC-60, as in previous works [9–13]. In the literature it can be seen that even in recent works some disagreements exist regarding the best point of the DSC curve to be associated to TTSS in the H–Zr solvus case, which has been subjected to intensive studies in the last decades [7–26].

Fig. 1 shows the DSC curve in the dissolution stage of a hydrided titanium sample containing 4.13 at.%. As it was strongly studied for the nuclear applied zirconium alloys [10–12,15–19,22–24], the end of the dissolution process can be related to the three points indicated in the curve of Fig. 1: the peak point, where a temperature commonly called peak temperature is measured (*pT*), the maximum slope change in the derived curve, where a maximum slope temperature is determined at an intermediate point (*msT*); and the completion point at the baseline recovery, where a completion temperature is determined (*cT*). As shown in Fig. 1, there is a 25–30 °C difference between *pT* and *cT*. This difference is similar to that observed in the Zircaloy-4 case and other zirconium alloys [10,12,15,18,20,24]. Since the correspondence between H–Ti and H–Zr systems in the solvus region is evident, our choice was to measure these three temperatures with the aim to compare the whole data set with the data existing in the literature for Ti–H [2–6].

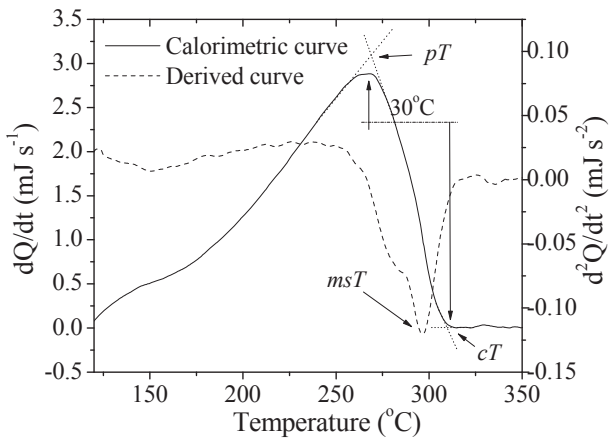

Fig. 1 – Calorimetric curve during dissolution (4.13 at.%). The points related to the TTSS determinations are indicated.

The DSC program consisted in three successive runs from room temperature to 340 °C (T_{max}) at a heating rate of 20 °C/min which produces a noiseless signal even for low concentration samples. However, this rate is higher than the commonly used for Ti–H solvus determinations [1–6]. It was not clear from the works consulted whether there are effects of heating rate on TTSS. Therefore an intensive study was made here to determine its influence, as was made for the H–Zr solvus in a previous work [10].

At each run the sample remained 5 min at T_{max} and then it was cooled at the same rate. The runs were made under a dynamic N_2 atmosphere (99.99%) of 25 ml/min. The samples were placed on platinum crucibles. An empty crucible was used as reference. No interference with the crucible has been detected.

Since the baseline has a non negligible slope, it was mathematically corrected to avoid any effect on TTSS measurements (Fig. 1).

X-ray diffraction experiments

The X-ray diagrams were obtained using two diffractometers. A Philips XPERT PW 3050, with a cooper anode ($\lambda_{K\alpha 1} = 1.540598$) and a graphite monochromator in the $\theta/2\theta$ layout with a scan step of 0.02° and a Philips PW3710, with a copper anode and a graphite monochromator too. The patterns were performed in the same θ-2θ layout with a scan step of 0.03°.

Influence of the heating rate on TTSS

In order to determine the solvus line of the Ti–H system with a thermal analysis technique as DSC, it is necessary to choose some criteria to select an adequate heating rate for the experiments. Although a low heating rate is desirable to produce experimental conditions next to thermodynamic equilibrium, low rates reduce the energy amount that must be detected per time unit generating conditions closer to the detection limit of the calorimeter; which produces a weak signal with considerable noise. On the other hand, if the rate is high, a similar energy amount will be absorbed in a shorter time, producing the opposite effect, i. e., a strong signal with a negligible noise. However, it is necessary to quantify if these conditions which are more distant from equilibrium have any significant effect on TTSS.

Please cite this article in press as: Vizcaíno P, et al., Terminal solid solubility determinations in the H–Ti system, International Journal of Hydrogen Energy (2015), http://dx.doi.org/10.1016/j.ijhydene.2015.06.058

There are divergences in previous works respect to the influence of the heating rate on TTSS. Köster's internal friction (IF) data indicate a systematic increase of 20 °C in TTSS varying the rate from 2.8 to 12 °C/min [2]. Paton (resistivity), in order to obtain equilibrium conditions, takes some minutes to equilibrate the system for T > 150 °C and some days for 25 °C (room temperature) [3]. Numakura (IF) does not find any dependence with heating rate in the range 0.2–4 °C/min [6]. Luo (DSC) determining the eutectoid transition temperature at 5, 10, 20 and 40 °C/min does not find any effect of heating rate on this temperature [5]. In the present context it was considered convenient to make a study of TTSS dependence with heating rate and, if it exists, to quantify it.

Comparison of heating rates

For this purpose we refer to two samples, A and B, of relatively high concentration, containing 1.38 at.% and 3.77 at.%, respectively. These samples were tested at the following heating rates: 2.5 °C/min, 5 °C/min, 10 °C/min and 20 °C/min. The DSC dissolution curves for both samples are shown in Figs. 2 and 3.

As can be observed in Figs. 2 and 3, the signals obtained at both 2.5 °C/min and 5 °C/min are very noisy. For sample A, a TTSS determination in a reliable form is virtually impossible. In Fig. 3 (sample B) TTSS can be measured but the error produced by noise is significant. Thus, this rate only allows to determine TTSS in the high hydrogen sample B. For the case of sample A, TTSS could not be determined. Additionally, it is interesting to note that in the curves of the Figs. 2 and 3 it is not observed any increasing tendency of TTSS with heating rate (*pT* values).

Analysis of variance

Fig. 2 shows that even at the curve obtained at 5 °C/min the noise superimposed is not negligible and raises TTSS error. Logically, this noise becomes more significant for low concentration samples where the dissolution signal is weaker.

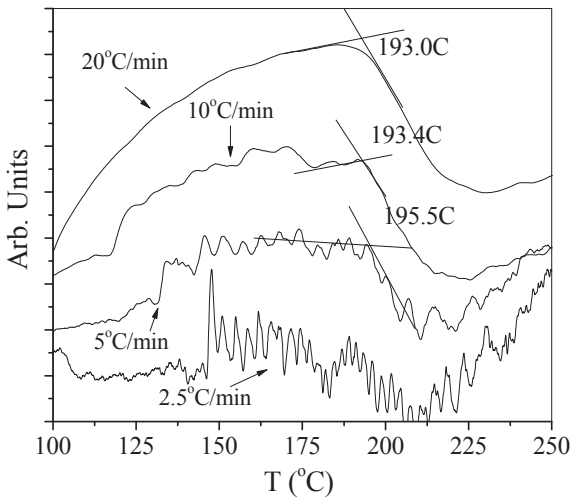

Fig. 2 – DSC curves for sample A (1.38 at.%) at the selected rates.

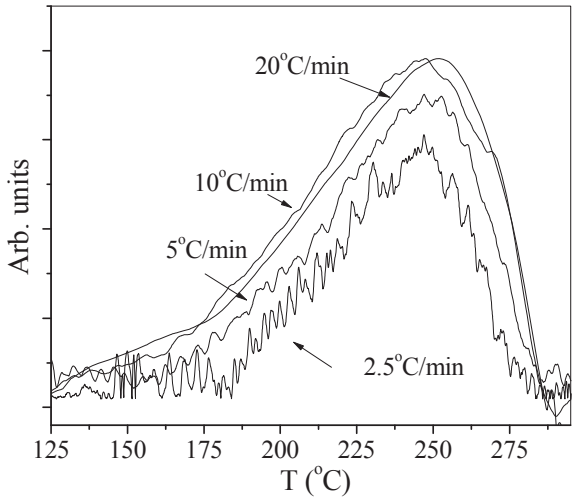

Fig. 3 – DSC curves for sample B (3.77 at.%) at the selected rates.

Inversely, the curves obtained at 20 °C/min are free of noise, showing the convenience to choose this rate. In order to asses the influence of the heating rate on TTSS the following experimental program was designed: four runs were performed to sample B at each one of the following rates: 5 °C/min, 10 °C/min and 20 °C/min. Between runs the sample remained at room temperature more than 24 h. The thermal cycle consisted in a heating up to 320 °C with 5 min remaining at this temperature and then a cooling at the same rate. Tables 2–4 show TTSS values determined from each run at *pT*, *msT* and *cT*, respectively.

Since at 5 °C/min or even at 10 °C/min in some cases the signal shows a non-negligible noise, it was considered more convenient to determine *pT* and *msT* by the tangents method, Fig. 2. In addition, the derivative of the DSC curve magnifies noise variations, which masks the maximum slope temperature, *msT*. Because this TTSS could not be determined in the runs performed at 5 °C/min. On the other hand, the curves obtained at 20 °C/min do not show any noise. Due to this TTSS was determined at the peak of the curve (*pT*) or the peak of its derivative (*msT*). The error is very small for these cases: 0.3–0.5 °C. The estimated errors are also indicated in the Tables 2–4

Thus, using TTSS data of sample B obtained at *pT* and *cT*, columns 1, 3 and 5 of Tables 2 and 4, a variance analysis of three data sets (columns) were conducted. Each column, assumed to be independent, is identified by a heating rate at its heading, which is the potential cause of variations on TTSS.

Table 2 – *pT* values for 5, 10 and 20 °C/min and estimated errors. Each value was determined from runs performed with sample B.

5 °C/min		10 °C/min		20 °C/min	
pT (°C)	ΔT (°C)	*pT* (°C)	ΔT (°C)	*pT* (°C)	ΔT (°C)
254.3	5.7	247.7	2.0	253.8	<0.5
247.4	4.4	250.6	2.4	251.7	<0.5
256.6	4.2	248.7	3.6	256.0	<0.5
260.1	3.4	247.6	2.0	259.4	<0.5

Please cite this article in press as: Vizcaíno P, et al., Terminal solid solubility determinations in the H–Ti system, International Journal of Hydrogen Energy (2015), http://dx.doi.org/10.1016/j.ijhydene.2015.06.058

Table 3 – *msT* values for 5, 10 and 20 °C/min and estimated errors. Each value was determined from runs performed with sample B.

5 °C/min		10 °C/min		20 °C/min	
msT (°C)	ΔT (°C)	*msT* (°C)	ΔT (°C)	*msT* (°C)	ΔT (°C)
Not determined		278.7	1.0	272.4	<1.0
		278.0	<0.5	282.3	<0.5
		280.5	<0.5	282.3	<0.5
		277.0	1.7	282.4	1.7

Table 4 – *cT* values for 5, 10 and 20 °C/min and estimated errors. Each value was determined from runs performed with sample B.

5 °C/min		10 °C/min		20 °C/min	
cT (°C)	ΔT (°C)	*cT* (°C)	ΔT (°C)	*cT* (°C)	ΔT (°C)
285.9	1.7	287.6	2.7	287.3	1.25
283.9	1.7	285.3	4.0	285.3	1.25
287.9	2.0	286.6	2.1	290.9	1.0
286.0	3.6	287.8	2.6	287.7	<1.0

The analysis resolves with a significance level of 0.05 if the sets are equal or not. The analysis compares the sum of the squared differences between the averages of the sets and the average of the population (Var_0) with the sum of the squared differences between the experimental data and the averages of the three data sets (Var_1). The ratio between these variances for a given level of significance (0.05) and degree of freedom of the data sets and population allows to calculate the Fisher function ($F_{calc} = Var_0/Var_1$), which is compared with its theoretical value to make a decision [27]. A theoretical value higher than the calculated implies that the differences between data sets are not significant. Table 5 shows these values.

From Table 5 it can be concluded that the three data sets belong to the same population. This means that under the experimental conditions in the analyzed heating rate interval we can assure, with a probability of 95%; that TTSS do not depend on heating rate. In other words, if the dependence with heating rate exists; the aleatory variations of the technique are more significant than this dependence, precluding its quantification. This behavior is similar to the one observed in the well-studied Zr–H solvus line [10]. From the previous analysis, TTSS can be determined on DSC dissolution curves obtained at 20 °C/min without any correction. Finally, since the thermocouple error (0.1 °C) is negligible compared with the statistical error, statistical error must be considered as TTSS error, that is: 1.7 °C for *pT*, 2.5 °C for *msT* and 1.2 °C for *cT*, in the high hydrogen concentration interval.

Table 5 – Results for the analysis of variance of three samples for *pT* and *cT* values.

	Variances				Fisher function	
	Var_0	d.f.[a]	Var_1	d.f.	$F_{calculated}$	$F_{theoretical}$
pT	52.7	2	13.8	9	1.13	4.26
cT	3.5	2	3.1	9	3.82	4.26

[a] d.f.: degree of freedom.

Joint results for the [α]/[α + γ] and [α]/[α + δ] boundaries

As indicated above, the temperatures of terminal solid solubility in dissolution were determined for each composition in the three points indicated in Fig. 1. Using TTSS data and the hydrogen concentration of the samples (X = H/Ti), the Van't Hoff plots were drawn and the linear regressions shown in Figs. 4–6 were obtained.

As seen in the plots, TTSS data are more disperse in the low hydrogen interval due to the low intensity of the DSC signal, which produces spread peaks, affecting the accuracy of the determinations.

From Van't Hoff plots the following equations were obtained for the whole data set:

For *pT* data:

$$\ln X = (-2679 \pm 58)/TTSS + (1.65 \pm 0.13); \quad (1)$$

For *msT* data:

$$\ln X = (-2800 \pm 64)/TTSS + (1.76 \pm 0.14); \quad (2)$$

For *cT* data:

$$\ln X = (-2819 \pm 63)/TTSS + (1.70 \pm 0.13); \quad (3)$$

where X is in atomic percent (at.%) and TTSS is in Kelvin.

Our results confirm that, within the working composition range, H–Ti behaves as an ideal system, adjusting to Van't Hoff law. Hence, the slopes of the regressions (1)–(3) give the solvus enthalpies. In addition, the interception with the pure Ti vertical axis (multiplied by ideal gas constant R) gives the solvus entropy. Both pairs of values are shown in Table 6.

It is important to mention that even though the system behaves as an ideal one, some deviation is observed between

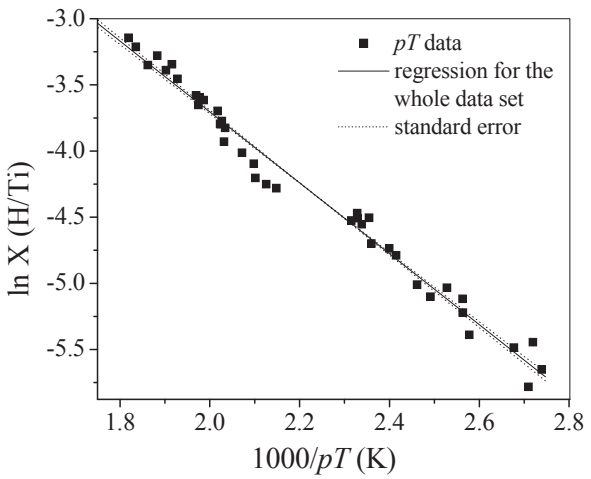

Fig. 4 – Van't Hoff plot drawn with *pT* values for the whole data set.

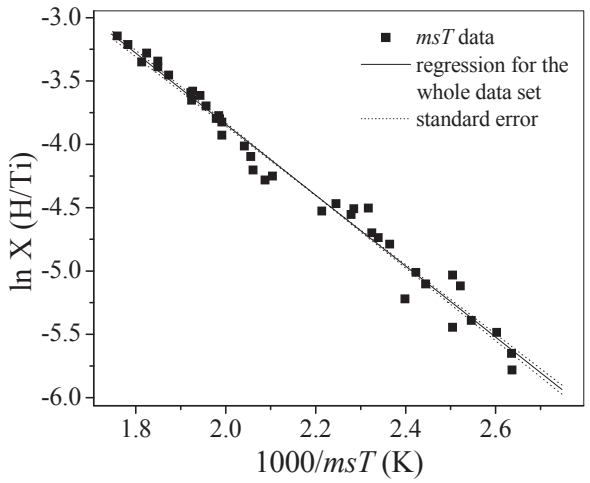

Fig. 5 – Van't Hoff plot drawn with *msT* values for the whole data set.

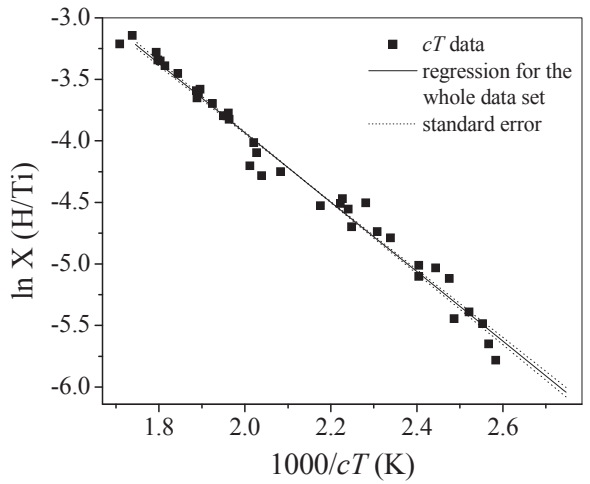

Fig. 6 – Van't't Hoff plot drawn with *cT* values for the whole data set.

the low-hydrogen interval (equilibrium [α]/[α + γ]), i.e., from 0.31 at.% to 1.15 at.% and the high concentration one (equilibrium [α]/[α + δ]), from 1.41 at.% to 4.13 at.%. This is clear in Fig. 4 (*pT* data) and suggests that the slope of the low concentration interval is smaller than the high concentration one. This change in the tendency is emphasized in Fig. 7 for TTSS values measured at *pT*, the criterion which produced the minor dispersion in the whole data set, but the same behavior is observed for *msT* and *cT* data. In this graph two regression lines for the low and high concentration intervals are plotted. Also, the enthalpy values obtained from each criterion for both concentration intervals are shown in Table 7.

Table 6 – ΔH_{solvus}, ΔS_{solvus} and errors.

	ΔH (kJ/molH)	ΔS (J/K molH)
pT	22.3 ± 0.5	13.8 ± 1.1
msT	23.4 ± 0.5	14.7 ± 1.2
cT	23.5 ± 0.5	14.2 ± 1.1

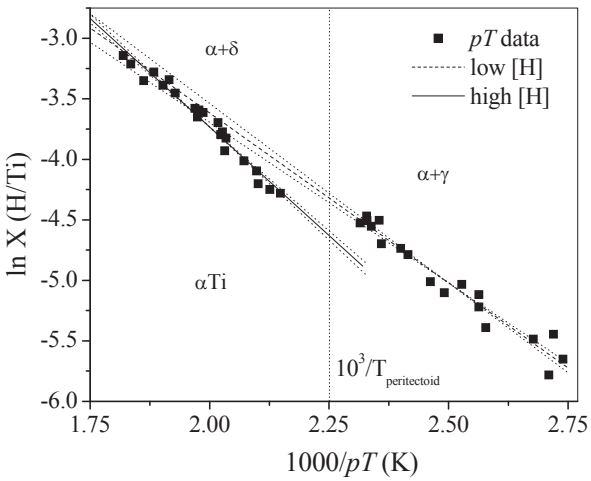

Fig. 7 – Van't Hoff. Plots for the low and high hydrogen composition ranges (*pT* data).

Fig. 8 shows a comparison between the data found in the literature for α–Ti and that of the present work. For this purpose data obtained at *pT* and *msT* were plotted, not *cT*. Regarding to the point where TTSS should be determined on the DSC curve, there were some discussions in the last decade related with the very similar H–Zr solvus line [9–12,15–20,22–24]. The author has observed that for the H–Zr system the best fit with equilibrium the Kearns and Zuzek's curves was found for *cT* values [10]. This is the reason why we have included *cT* data in the present work, Fig. 6. However, two relatively recent experimental works arrived to different conclusions: Khatamian and Root [22] and Khatamian [24] using DSC and neutron diffraction as a contrasting technique concluded that the most representative point of TTSS is *pT*. In a previous work, Pan and Puls [17], performing quasistatic thermal cycles and determining by the elastic modulus changes with temperature the dissolution and precipitation temperatures concluded that the best point to associate TTSS is *msT*. The most physically clear paper seems to be the Khatamian's ones [24] but, in any case, the reliability of the conclusion from any of both papers is strongly related with the accuracy of the contrasting technique: neutron diffraction cannot resolve precipitates smaller than a hundred of nanometers and internal friction (Pan's work, [17]) is capable to detect displacements of atoms to vacant sites in the lattice, that is, much smaller objects. We have commented on these topics in Ref. [23].

It is interesting to mention here that the intrinsic anisotropy of the hexagonal metals like Ti and Zr plus the crystallographic texture (developed during the metallurgical processing) have effects on the hydride dissolution/

Table 7 – ΔH_{solvus} for the low and high hydrogen intervals with their errors.

	ΔH_{low} (kJ/molH)	ΔH_{high} (kJ/molH)
pT	23.4 ± 1.3	29.9 ± 1.2
msT	25.1 ± 2.0	28.0 ± 1.1
cT	23.2 ± 1.8	24.1 ± 1.2

Please cite this article in press as: Vizcaíno P, et al., Terminal solid solubility determinations in the H–Ti system, International Journal of Hydrogen Energy (2015), http://dx.doi.org/10.1016/j.ijhydene.2015.06.058

precipitation process which can explain part of the differences observed between the points associated to TTSS in the calorimetric curve. Recent hydride dissolution/precipitation experiments in the nuclear alloy Zr-2.5Nb performed in situ using synchrotron light shown that it can be defined a TTSS for each one of the main texture components of the microstructure [26]. In this work it was found that these TTSS values can differ up to 20 °C due to the different stress state of these components [26]. Since the DSC technique only "sees" bulk average effects, the different behavior of the texture components only could be registered as a delay in the baseline recovery producing the observed differences between the minimum (*pT*) and the completion points (*cT*).

In any case, at present the unique works performed to find the physical point for TTSS on the calorimetric curve are the one of Khatamian [24], which gives evidence in favour of *pT* and the one of Pan [17], which gives evidence in favour of *msT*. In the present context we will make the comparison between these data with which can be found in the bibliography.

Discussion

Comparison with previous data in the literature

As shown in Fig. 8, the agreement with the equilibrium data of Vitt [4] is good. The hydrogen interval of Vitt's work varies between 0.24 at.% and 1.44 at.%. This is just about the low hydrogen range of the present work. The enthalpy value obtained by Vitt is 18.8 kJ/molH, smaller in general than the values obtained in the present work but closer to the low hydrogen region ones, Table 7. An average curve made by Vitt [4] adding the Köster [2] and Paton [3] dissolution sets is also plotted in Fig. 8. The enthalpy value of this fit is 21.0 kJ/molH, higher than 18.8 kJ/molH, value obtained independently by Paton and Vitt in the low hydrogen interval. Since almost all of their data do not exceed 1.4 at% and TTSS values of these data are smaller than 168 °C, it could be assumed that these data corresponds to the dissolution of the γ hydride.

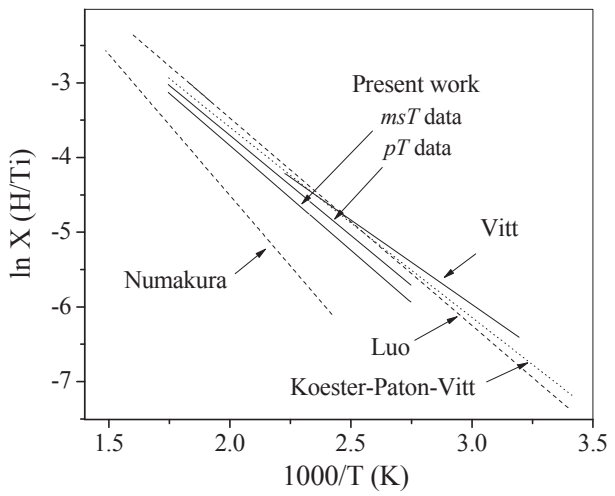

Fig. 8 – Comparison between the literature and the present work data: TTSS values measured at *pT* and *msT*.

Luo [5] contributes to the solvus with a couple of calorimetric values obtained from samples containing more than 3 at.%, and calculates the solvus line using Vitt, Paton and Köster data, but considering both, precipitation and dissolution data. Luo obtained an enthalpy value of 22.9 kJ/molH which is also similar to the values shown in Table 6. Luo's solvus line and also his solvus enthalpy calculated in this manner are probably affected by hysteresis. However, Luo's work is taken as a reference work together with that of Köster, Paton and Vitt concerning the solvus in the Ti–H diagram because of the consistency between his data and the previous ones to be aligned in a straight line in the Van't Hoff plot [1].

On the other hand, Numakura's [6] dissolution data obtained by internal friction show the greatest shift regarding to the present work and literature data. The hydrogen range of this work varies from 0.5 to 7 at%, but most of the data corresponds to concentrations higher than 3 at.%. As was verified in the present work and as found in literature, in this range it is difficult to obtain γ phase [1]. Since these data have the main weigh in Numakura's Van't Hoff plot, it is reasonable to think that the high enthalpy value of 31.5 kJ/molH found by Numakura should be mostly due to the dissolution of the δ hydride.

At this point it is interesting to observe the enthalpy values shown in Table 7 for the low hydrogen interval (0.3 at.%–1.4 at.%) and the high hydrogen one (1.4 at.%–4.1 at.%) obtained from our data performing Van't Hoff plots like the observed in Fig. 7. The values calculated from the low hydrogen interval are similar to the Vitt, Paton and Köster ones, but the values of the high hydrogen interval are close to the Numakura's value. It is evident to tie this behavior to the dissolution reactions γ + αTi → αTi (H) for the low concentration interval and δ + αTi → αTi (H) for the high concentration one.

Some thoughts emerge from the analysis: Luo's data provided a couple of high concentration values, which were merged with previous data provided by Köster, Paton and Vitt [2–4]. In this complete data set the amount of low (i.e. <1.4 at.%) and high concentration (>1.4 at.%) data are almost similar, the low concentration data being more disperse than the rest [5]. The complete data set of the present work is much larger than Luo's one. It may be that our data were obtained from a unique technique (DSC), they are less dispersed in both sides of the solubility interval. These conditions allow us to perceive, which is not possible or at least not completely clear from Luo's data, the different tendencies between low and high hydrogen contents. However, if we consider the data of the present work as a unique interval, these tendencies are compensated and a solvus enthalpy value identical to Luo's one is calculated, 22.8 ± 0.5 kJ/molH (average *pT* and *msT* Van't Hoff slopes of Table 6).

The solvus enthalpies shown in Table 7 were calculated considering two hydrogen intervals, based on the TTSS criteria indicated in Fig. 1. Even though the values fluctuate depending on the selected criteria, ΔH_{solvus} in the low H interval is always smaller than in the high H interval. Even if the interception between the lines assessing the low hydrogen and the high hydrogen data occurs above the peritectoid temperature, it is difficult to ignore the different slopes observed in Fig. 7. We believe that this behavior is due to the

Please cite this article in press as: Vizcaíno P, et al., Terminal solid solubility determinations in the H–Ti system, International Journal of Hydrogen Energy (2015), http://dx.doi.org/10.1016/j.ijhydene.2015.06.058

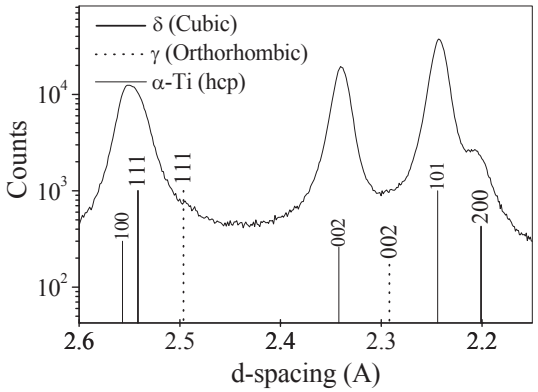

Fig. 9 – Diagram of a sample containing 5.0 at.%. It was annealed at 155 °C for a week. Only the δ peaks (111) and (200) are observed.

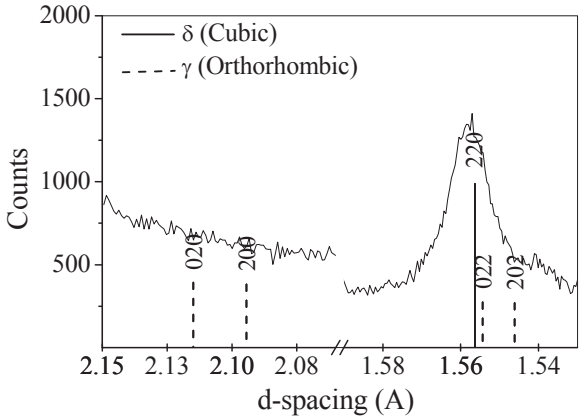

Fig. 10 – Diagram of a sample containing 11.0 at.%. It was cooled from 400 °C in furnace. Only the δ peak (220) is observed.

presence of small amounts of δ phase in the α + γ field. This interpretation is based on the fact that even though γ is the equilibrium phase at room temperature; the peritectoid reaction α + γ → α + δ is only partially reversible. Then it is difficult to obtain only γ hydrides in spite of the method applied for hydrogen incorporation [1]. Perhaps for the same reason the peritectoid reaction cannot be identified during a calorimetric run (heating) for high hydrogen samples, since the main fraction of hydride phase is δ in these samples. This is not the case for low hydrogen samples, where γ should be the majority phase [1].

Thus, the no-interception of the partial TTSS lines at the peritectoid temperature can be attributed to the metastable presence of small amounts of δ phase in the low hydrogen samples. This affects the [α]/[α + γ] equilibrium, slightly increasing the hydrogen content of the α phase. This picture was verified in the present work by X-ray diffraction.

Analysis of the X-ray diffraction data

In order to confirm the hypothesis which emerges from calorimetric data, many diffraction patterns of samples with different hydrogen contents and thermal treatments were made.

Fig. 9 shows a diffraction pattern of a sample with a concentration of 5.0 at.%. The positions of the most intense peaks of γ and δ phases[1] are indicated by bars in terms of the d-spacing [1,28]. The specimen was annealed at 155 °C for a week to favor the γ hydride formation. However, only the peaks $(111)_\delta$ and $(200)_\delta$ of the δ phase are observed, not that of the γ phase, which agrees with the assumption that the reaction α + γ → α + δ is at least only partially reversible [1].

Figs. 10 and 11 show the diffraction patterns obtained for a sample of 11.0 at.%. The diagrams show a d-spacing region where the positions of four peaks of γ and one of δ phases are indicated, relatively isolated from the α-Ti peaks. The pattern of Fig. 10 corresponds to a sample cooled in furnace from 400 °C. In the diagram only the peak $(220)_\delta$ is observed. Fig. 11 shows the same region for a powder obtained from the sample of Fig. 10 (11.0 at.%) but annealed at 600 °C and quenched in air. At the positions of the γ peaks $(020)_\gamma$ and $(200)_\gamma$, an incipient distorted peak is observed. In both cases the annealing temperatures were above the eutectoid reaction α + δ → α + β. Only in the quenched specimen the γ hydride is observed, possibly due to the limiting effect on the diffusion forced by quenching. Similar behavior was observed in hydrided Zircaloy quenched from temperatures above the eutectoid reaction of this system (550 °C) [29].

Finally, for a sample with hydrogen content of 0.55 at.%, the hydride mainly observed is γ. In Fig. 12, the peak $(111)_\gamma$ is the unique hydride peak clearly developed, even though some slight distortion at the right side of the αTi peaks (100) and (101), where the δ peaks (111) and (200) are located, indicate the possible presence of metastable δ phase. Thus, from both, DSC and XRD data, the most reasonable interpretation of the change in the slope of the solvus line seems to be the presence of the γ phase in the low hydrogen interval. In this case, the slopes consigned in Table 7 corresponds to the solvus

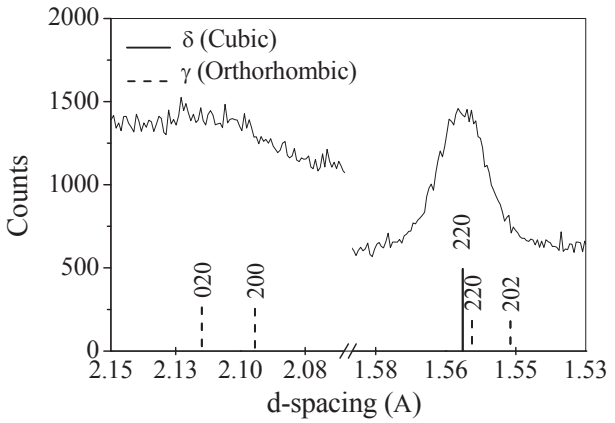

Fig. 11 – Powder diagram. The sample contains 11.0 at.%, and was cooled from 600 °C in air. An incipient γ distorted peak (020) is observed.

[1] The crystalline structure considered here for the phase γ is the accepted in the last revision of the Ti–H Equilibrium Diagram [1,28].

Please cite this article in press as: Vizcaíno P, et al., Terminal solid solubility determinations in the H–Ti system, International Journal of Hydrogen Energy (2015), http://dx.doi.org/10.1016/j.ijhydene.2015.06.058

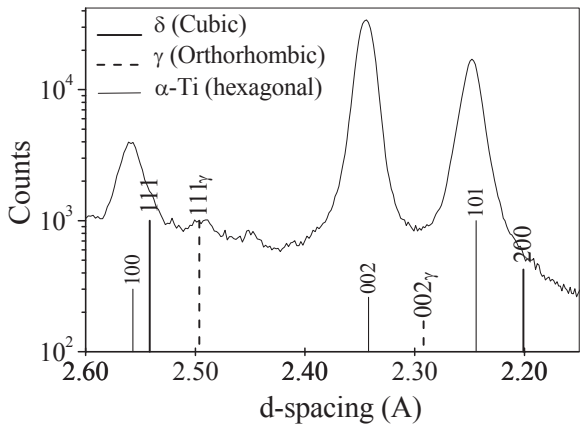

Fig. 12 – Diagram of a sample containing 0.55 at.%, cooled from 250 °C at 1 °C/min. The γ (111) hydride peak is observed but in addition some distortion at the right side of the αTi peaks (100) and (101) at the position of the δ peaks (111) and (200), respectively, suggest small amounts of metastable δ phase.

enthalpies of the $\gamma + \alpha \rightarrow \alpha$ (low hydrogen) and $\delta + \alpha \rightarrow \alpha$ (high hydrogen) transformations, which evidence the peritectoid reaction $\alpha + \gamma \rightarrow \alpha + \delta$, as was observed in the quite similar H–Zr system for the same reaction [30].

Eutectoid reaction

Fig. 13 shows the calorimetric curve of a sample with a hydrogen content of 11.0 at.%. In this sample and others of similar concentrations the temperature of the hydride decomposition in the eutectoid reaction $\alpha + \delta \rightarrow \alpha + \beta$ was measured. Averaging the values obtained from three samples, 319.9 ± 1.9 °C was obtained for T_{eutec}. The intersection between the horizontal line [αTi + δ]/[αTi + βTi] at 319.9 °C and the solubility curves obtained from equations (1) and (2) (*pT* and *msT* fits, respectively) gives an average value of 5.44 ± 0.27 at.% for the ending of the boundary limit [α]/[α + δ], Fig. 14.

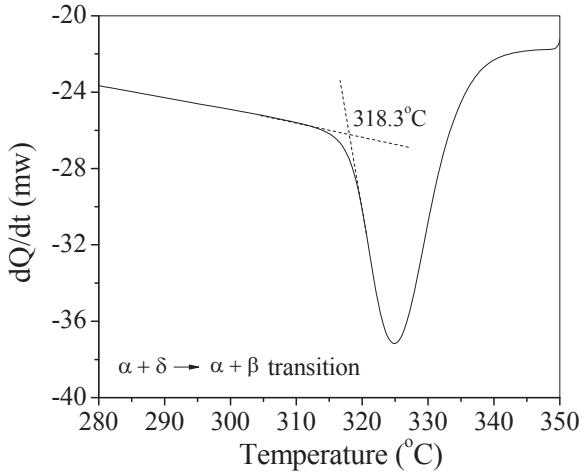

Fig. 13 – Calorimetric curve of the hydride decomposition reaction $\alpha + \delta \rightarrow \alpha + \beta$ (during heating). The sample contains 11.0 at.%.

Conclusions

The solvus line of hydrogen in α-Ti was determined by differential scanning calorimetry. A set of 43 samples with concentrations ranging from 0.3 at.% to 4.1 at.% were measured. Averaging the TTSS solubility values obtained from *pT* and *msT* points in DSC diagrams, the following relation was established:

$$\ln X = (2740 \pm 70)\ 1/\mathrm{TTSS} + (1.71 \pm 0.25)$$

where $0.3 \leq X \leq 4.1$ at % H and TTSS ranges from 369 K (96 °C) to 593 K (320 °C).

The solvus enthalpy calculated using the previous equation is

$$\Delta H = 22.8 \pm 0.5\ \mathrm{kJ/molH}.$$

More in detail, we found that the solvus line behaved in two different ways according to the hydrogen content, that is X > 1.4 at.% and X < 1.4 at.%. In the high concentration range there is the [α/α + δ] equilibrium boundary while in the low concentration range the boundary corresponds to the [α/α + γ] equilibrium coexistence probably slightly modified by the presence of small amounts of the metastable δ phase retained upon cooling. We detected this remaining δ phase by means of X-ray diffraction measurements made on heat treated samples. These X-ray measurements also confirmed that the presence of the metastable δ phase was responsible for the reaction $\alpha + \gamma \leftrightarrow \alpha + \delta$ not being strictly reversible at the peritectoid temperature. It was only at the low H concentrations, X < 0.55 at.%, were we found the pure α + γ equilibrium coexistence.

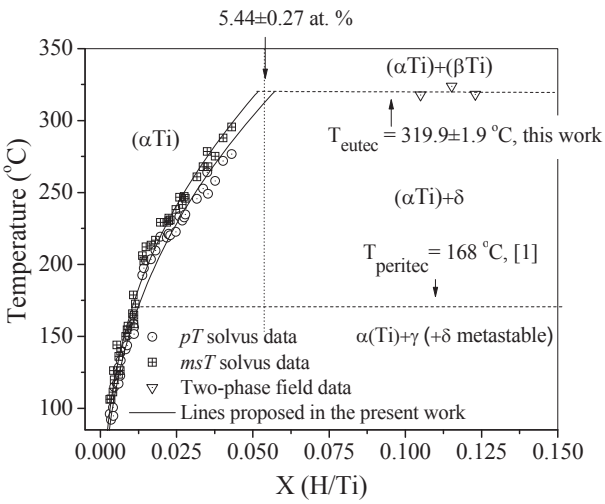

Fig. 14 – Solvus and end of the boundary limit [α]/[α + δ] for the H–Ti system.

Please cite this article in press as: Vizcaíno P, et al., Terminal solid solubility determinations in the H–Ti system, International Journal of Hydrogen Energy (2015), http://dx.doi.org/10.1016/j.ijhydene.2015.06.058

Using high concentration samples (9.5 at.%–11.0 at.%) we have also determined the eutectoid $\beta \leftrightarrow (\alpha + \delta)$ decomposition temperature. The result obtained was 319.9 ± 1.9 °C. By extrapolation of the $[\alpha]/[\alpha + \delta]$ solubility curve up to this temperature we found that at this eutectoid reaction the solubility of H in α-Ti is 5.44 ± 0.27 at.%.

Acknowledgements

The authors are grateful to Lic. Guillermo Cozzi, from the Servicio Geológico Minero Argentino (SEGEMAR), and Dr. Daniel Vega, from the Comisión Nacional de Energía Atómica (CNEA), for their support in the X-ray measurements. In addition we would like to thank to Prof. Javier Palmerio for the hydrogen measurements.

The original material was provided by the metallurgical company FAE.SA, Ezeiza, Argentina.

REFERENCES

[1] Manchester FD, San Martín A. Phase diagrams of binary hydrogen alloys. Monograph Series on Alloy Phase Diagrams. Ohio USA. 2000.
[2] Köster W, Bangert L, Evert M. Z Metallkunde 1956;47:564–70.
[3] Paton NE, Hickman BS, Leslie DH. Metall Trans 1971;2:2791–6.
[4] Vitt RS, Ono K. Metall Trans 1971;2:608–9.
[5] Luo W, Flanagan TB, Clewley JD, Dantzer P. Metall Trans A 1993;24:867–73.
[6] Numakura H, Koiwa M. Trans Jpn Inst Metals 1985;26(9):653–62.
[7] Puls MP. Acta Metall 1984;32(8):1259–69.
[8] Puls Manfred P. The effect of hydrogen and hydrides on the integrity of zirconium alloy components. ISSN 1612–1317 ISSN 1868-1212 (electronic). ISBN 978-1-4471-4194-5 ISBN 978-1-4471-4195-2 (eBook). London: Springer-Verlag; 2012. http://dx.doi.org/10.1007/978-1-4471-4195-2. Springer London Heidelberg New York Dordrecht. Library of Congress Control Number: 2012940465.
[9] Vizcaino P, Banchik AD, Abriata JP. J Nucl Mater 2002;304:96–106.
[10] Vizcaíno P, Banchik AD, Abriata JP. Metall Mater Trans A 2004;35A(8):2343–9.
[11] Vizcaino P, Banchik AD, Abriata JP. J Nucl Mater 2005;336:54–64.
[12] Vizcaino P, Rios RO, Banchik AD. Thermochim Acta 2005;429:7–11.
[13] Vizcaíno P, Flores AV, Bozzano PB, Banchik AD, Versaci RA, Ríos RO. J ASTM Int 2011;8:1–20.
[14] Pan ZL, Ritchie IG, Puls MP. J Nucl Mater 1996;228:227–37.
[15] Khatamian D, Ling VC. J Alloys Compd 1997;253–254:162–6.
[16] Khatamian D. J Alloys Compd 1999;293–295:893–9.
[17] Pan ZL, Puls MP. J Alloys Compd 2000;310:214–8.
[18] McMinn A, Darby EC, Schofield JS. Zirconium in the nuclear industry: twelfth international symposium. ASTM STP 2000;1354:173–95.
[19] Une K, Ishimoto S. J Nucl Mater 2003;322:66–72.
[20] Khatamian D. J Alloys Compd 2003;356–357:22–6.
[21] Singh RN, Mukherjee S, Gupta Anuja, Banerjee S. J Alloys Compd 2005;389:102–12.
[22] Khatamian D, Root JH. J Nucl Mater 2008;372:106–13.
[23] Giroldi JP, Vizcaíno P, Flores AV, Banchik AD. J Alloys Compd 2009;474:140–6.
[24] Khatamian D. J Nucl Mater 2010;405:171–6.
[25] Zanellato O, Preuss M, Buffiere JY, Ribeiro F, Steuwer A, Desquines J, et al. J Nucl Mater 2012;420:537–47.
[26] Vizcaíno P, Santisteban JR, Vicente Alvarez MA, Banchik AD, Almer J. J Nucl Mater 2014;447:82–93.
[27] Devore Jay L. Probability and statistics for engineering and the sciences. Belmont, California 94002: Books/Cole Publishing Company. Wadsworth, Inc.; 1982.
[28] Numakura H, Koiwa M, Asano H, Izumi F. Acta Metall 1988;36:2267–73.
[29] Nath B, Lorimer GW, Ridley N. J Nucl Mater 1975;58:153–62.
[30] Root JH, Small WM, Khatamian D, Woo OT. Acta Mater 2003;51:2041–53.

Please cite this article in press as: Vizcaíno P, et al., Terminal solid solubility determinations in the H–Ti system, International Journal of Hydrogen Energy (2015), http://dx.doi.org/10.1016/j.ijhydene.2015.06.058